

Vertical transport in all-binary GaAs/AlAs short-period superlattices and carrier trapping and detrapping dynamics by different quantum wells

K. Fujiwara^{*1}, A. Satake¹, L. Schrottke², R. Hey², and H. T. Grahn²

¹ Department of Electrical Engineering, Kyushu Institute of Technology, Tobata, Kitakyushu 804-8550, Japan

² Paul-Drude-Institute for Solid State Electronics, Hausvogteiplatz 5-7, 10117 Berlin, Germany

Received ZZZ, revised ZZZ, accepted ZZZ

Published online ZZZ

PACS 73.50.Gr, 78.47.+p, 78.66.Fd, 78.67.Pt, 73.21.Cd, 78.55.Cr

Dynamics of vertical transport in all-binary GaAs/AlAs short-period superlattices (SPSs) have been investigated as a function of temperature by steady-state and time-resolved photoluminescence (PL) experiments. When two different, enlarged quantum wells are embedded in the SPSs, photoexcited carriers compete to be trapped into various localized exciton states and a variety of exciton radiative recombination dynamics appears accompanied by phonon heating. Redistribution of carrier population in the different wells by phonon scattering is significantly influenced by vertical miniband transport in the SPSs. Three different transport regimes are pointed out: (i) tunneling transport affected by irreversible carrier cooling into deep localized states, (ii) interplay of carrier relaxation and phonon-assisted activation mediated by an efficient miniband Bloch transport, and (iii) thermalization processes.

copyright line will be provided by the publisher

1 Introduction

The concept of short-period superlattices (SPSs) proposed almost two decades ago is very useful to improve material qualities of quantum well heterostructures [1-5]. This is especially true, when such all-binary GaAs/AlAs SPSs replace AlGaAs ternary alloy barriers and/or cladding layers in laser structures [6-8]. From a growth point of view, AlGaAs alloys are inherently heterogeneous, since Ga-As and Al-As bond energies are different in the AlGaAs alloy, while there are no such constraints on all-binary GaAs/AlAs SPSs when used as digital alloys. Therefore, very low threshold current densities for lasing as low as 200 A/cm² have been achieved for separate-confinement-heterostructure lasers [6], since the internal quantum efficiency is drastically improved [9]. SPSs with superior heterointerface properties are also useful for various electronic devices which utilize tunnelling transport properties, as discussed in books and review papers [10-13]. The concept of SPSs is extensively utilized also to InGaN materials as strained layer superlattices for blue lasers [14] and light-emitting diodes [15]. Concerning semiconductor superlattices in general, a very large number of papers have previously been reported to date to study vertical transport in superlattices consisting of a variety of compound semiconductor materials. These may be found in various review books like the one edited by Holger T. Grahn [10]. Recently, the carrier transport in quantum cascade laser structures [16] as well as Bloch oscillations [17] have been under active investigation. However, these topics are beyond the scope of this study, and we will concentrate on all-binary GaAs/AlAs SPSs, as a prototype superlattice system.

* Corresponding author: e-mail: fujiwara@ele.kyutech.ac.jp, Phone: +81 93 884 3221, Fax: +81 93 884 0879

copyright line will be provided by the publisher

One of the attractive means to investigate the vertical carrier transport along the growth axis in SPSs by optical spectroscopy is to use an “enlarged well” [2, 11, 12]. In a SPS with an enlarged quantum well (QW) intentionally introduced, photoexcited carriers sink into the enlarged well across the SPS. This vertical motion of the carriers from the SPS to the enlarged well has previously been observed by means of both steady-state and time-resolved photoluminescence (PL) spectroscopy. In previous PL experiments [18-20], for example, it has been shown, that with increasing temperature, the vertical transport processes in SPSs change from an incoherent tunnelling-assisted hopping conduction to Bloch-type conduction. Furthermore, the crossover point from tunnelling-assisted hopping conduction to Bloch-type transport critically depends on the barrier thickness [19]. An enlarged QW, incorporated into a system of SPSs, acts as a carrier localization centre, in which the carriers may recombine. Such a system can be considered as a band-engineered semiconductor heterostructure that allows us to test the transport properties of a system containing localized states, which are formed by subbands in QWs, and extended states provided by minibands in SPSs. In this case, the localization energy (i.e., potential depth) is controlled by the thickness of the enlarged well.

In this paper, we discuss the vertical transport properties of photoexcited carriers between two GaAs QWs with different well thicknesses embedded in GaAs/AlAs SPSs investigated in detail by optical spectroscopy [21]. The existence of two carrier localization centres allow us to study the interplay of carriers occupying states in the SPS as well as in the two localization centres, since their PL signals are well spectrally discriminated. We have extensively studied the PL dynamics of this interesting system as a function of temperature to extract information concerning radiative recombination properties as well as carrier trapping and detrapping dynamics.

2 Experimental

The sample used for this study was grown on a GaAs (100) substrate by molecular-beam epitaxy (MBE). The layered heterostructure is schematically shown in Fig. 1. On top of a GaAs buffer layer with a thickness of 600 nm, an all-binary GaAs/AlAs SPS (SPS1) layer sandwiched between a pair of two other GaAs/AlAs SPSs (SPS2, containing 130 periods at the substrate side and 57 periods at the surface side) was grown. The well and barrier thicknesses in SPS1 (SPS2) are 4.9 nm (2.3 nm) and 1.0 nm (1.0 nm), respectively. Within SPS1, three GaAs layers were enlarged or shrunk to 7.8 nm (QW1), 5.5 nm (QW2), and 3.5 nm (QW3), which serve as localization centres (sinks) or an unbound state for photoexcited electrons and holes to monitor the degree of the tunnelling and capture efficiency. These QWs are separated by 6-period SPS1s and confined by a pair of 12-period SPS1s. For the QWs, 2-min growth interruption was carried out at the GaAs well interfaces under arsenic flux exposure. The complete structure is capped by a 3.5 nm thick GaAs layer.

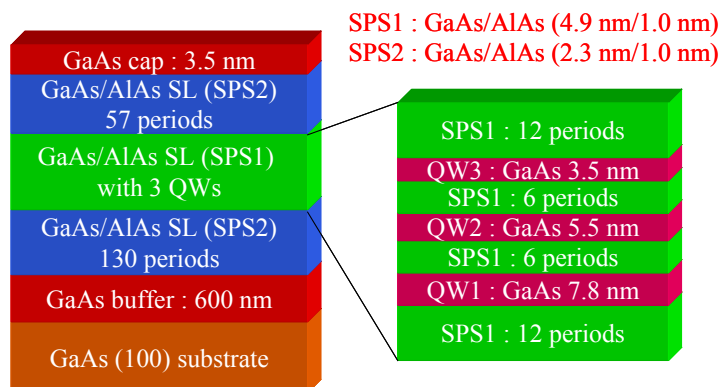


Fig. 1 Schematic diagram of layered sample structure.

The sample was investigated by PL as well as PL excitation (PLE) spectroscopy. Steady-state PL spectra were measured between 15 and 300 K in a closed-cycle He cryostat using a He-Ne laser (2.4 mW power) at 632.8 nm for excitation and a computer controlled digital lock-in amplifier system employing a 0.32-m monochromator and a GaAs photomultiplier for ac detection. High-resolution PLE spectroscopy [22] was used to investigate absorption properties at 5 K in a flow cryostat. For this purpose, the PL signal was dispersed in a 1-m monochromator and detected with a liquid-nitrogen cooled charge-coupled-device detector. The optical excitation was carried out with a tunable Ti:sapphire laser pumped by an Ar⁺ laser. The PL spectra were recorded as a function of the excitation energy using 1 nm (about 2 meV) steps. Spectrally and temporally resolved PL transients were measured between 20 and 300 K in a closed-cycle He cryostat using a diode laser at 653 nm with 50 ps pulses for weak excitation (average power of 1 μW) and a streak camera system for photon counting detection.

3 Results and Discussion

3.1 Low temperature PL/PLE

Figure 2 shows a PL spectrum recorded at 20 K by using the He-Ne laser with an excitation power of ~2.4 mW, i.e., an estimated power density of ~10 W/cm². The excitation wavelength corresponds to an energy of 1.96 eV. Four emission bands corresponding to QW1, QW2, SPS1, and SPS2 are clearly observed at about 1.592 eV, 1.640 eV, 1.663 eV, and 1.887 eV, respectively. We attribute the PL lines to the ground heavy-hole (1HH) exciton transitions associated with the subbands and minibands. For comparison, inter-band transition energies for QW1 and QW2 are calculated based on the envelope function approximation. As indicated in Fig. 2 by arrows, they are in good agreement with the experimental values. For the QW1 and QW2, we note that PL fine structures are additionally observed, which result from the formation of growth islands within the QW lateral planes due to growth interruption [23]. Under weak excitation, PL splitting is observed for QW1 (QW2) with an energy of 4.1 meV (8.0 meV) (see Fig. 3). The experimental value for QW1 (QW2) agrees with the value of 3.9 meV (8.5 meV) calculated for QW thickness differences of one monolayer.

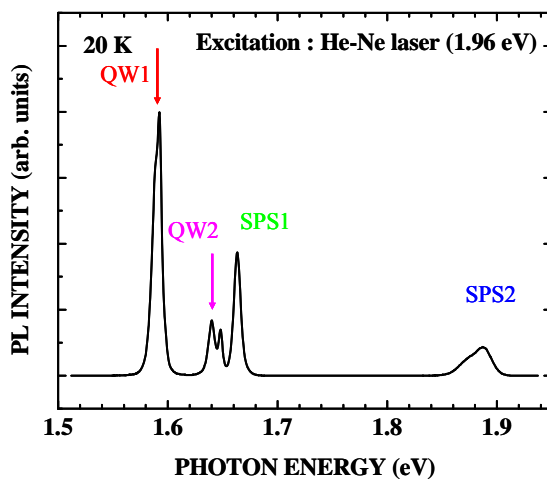


Fig. 2 PL spectrum at 20 K.

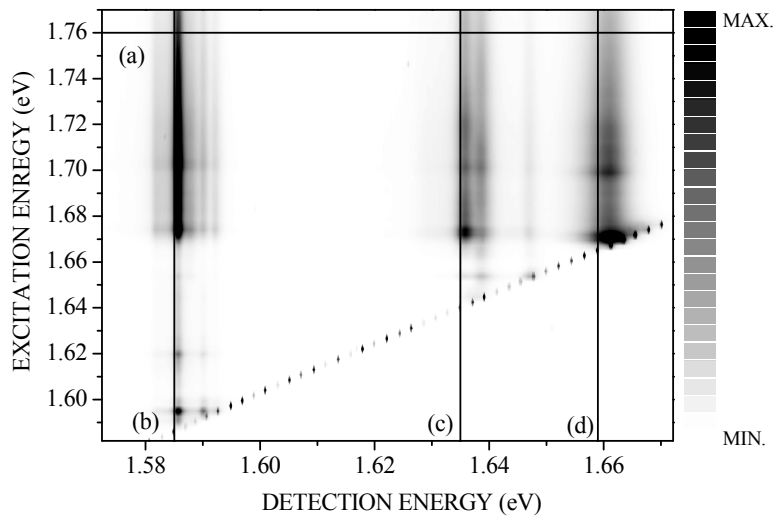


Fig. 3 Grey-scale plot of PL intensity as a function of excitation and detection energy at 5 K. The laser power for excitation is fixed to be $0.5 \mu\text{W}$.

In order to confirm our assignment of the PL transitions we have measured a series of high-resolution PL spectra by finely changing the excitation wavelength of the Ti-sapphire laser. As a result, the PL intensities are plotted in Fig. 3 using a grey scale representation as a function of detection and excitation energy. In this plot a horizontal cut corresponds to a PL spectrum for a fixed excitation energy and a vertical one to a PLE spectrum at a fixed PL detection energy. As an example, a PL spectrum (a) at 1.76 eV excitation and PLE spectra (b), (c), and (d) at detection energies of 1.585, 1.635, and 1.658 eV, respectively, are plotted in Fig. 4. We attribute the PL transition observed at about 1.66 eV to SPS1 and the

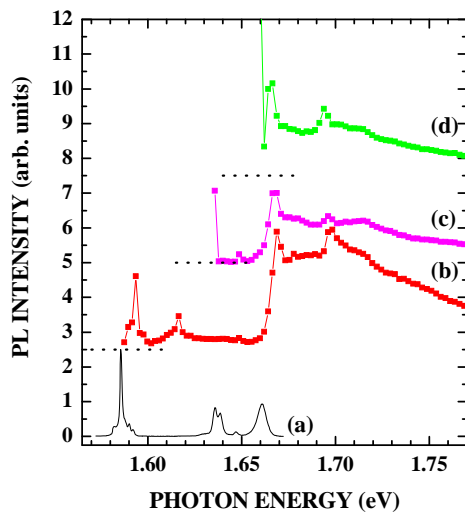


Fig. 4 (a) PL spectrum excited at 1.76 eV and PLE spectra detected at energies of (b) 1.585, (c) 1.635, and (d) 1.658 eV.

copyright line will be provided by the publisher

PL peaks observed around 1.58-1.59 and 1.635-1.648 eV to QW1 and QW2, respectively, which are Stokes-shifted from the 1HH excitonic resonance lines of QW1 and QW2. Note that the PL doublet shown in Figs. 2-4 for QW2 with a splitting of ~ 3 meV may be attributed to the coexistence of free and localized excitons [24-26] belonging to the same growth island. From the PLE spectra (b)-(d) the 1HH exciton resonance as well as the ground light-hole (1LH) resonance peaks for QW1 and SPS1 are clearly observed. Furthermore, we can estimate the energy difference between 1HH and 1LH resonances from the PLE spectra (b) and (d) shown in Fig. 4 to be 23 meV (29 meV) for QW1 (SPS1), in good agreement with the theoretically calculated value of 25 meV (30 meV). Note that the PL emission intensity of QW1 is much larger than the one of QW2 when the sample is excited at the band edge of SPS1. Therefore, we conclude that the deeper QW1 rather efficiently captures photoexcited carriers from the miniband of SPS1. This finding is consistent with the PL result shown in Fig. 2. The high-resolution PLE spectra demonstrate that the eigen-energy states of the wide (QW1) and the narrow (QW2) wells embedded in SPS1 are related to well-defined PL bands. Therefore, the QW states can be utilized as carrier trapping centres to monitor the vertical transport in the SPS1.

3.2 Temperature dependence of PL spectra

Figure 5 shows steady-state PL spectra of the sample for temperatures between 15 and 300 K, excited by the cw He-Ne laser. When the sample temperature is increased from 15 K to higher temperatures, the PL lines exhibit a general red-shift with increasing temperature following the temperature dependence of the GaAs band gap [27]. For temperatures below 50 K, the PL emission intensities of QW2, SPS1, and SPS2 drastically decrease for increasing temperature, while the PL intensity for QW1 increases significantly, reaching the maximum value at 60 K. Above 120 K, on the other hand, the PL signal from the SPS1 reappears after its complete disappearance at about 80 K and its intensity increases progressively with

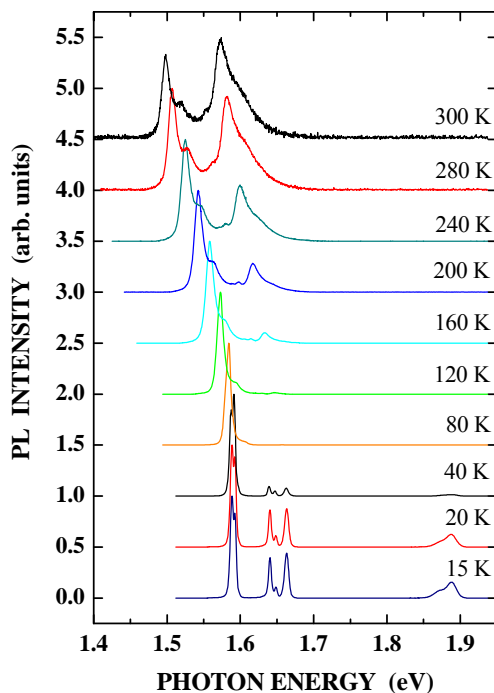


Fig. 5 Temperature dependence of PL spectra between 15 and 300 K. For each spectrum, the PL intensity is normalized to the maximum value and the base line is vertically shifted for clarity.

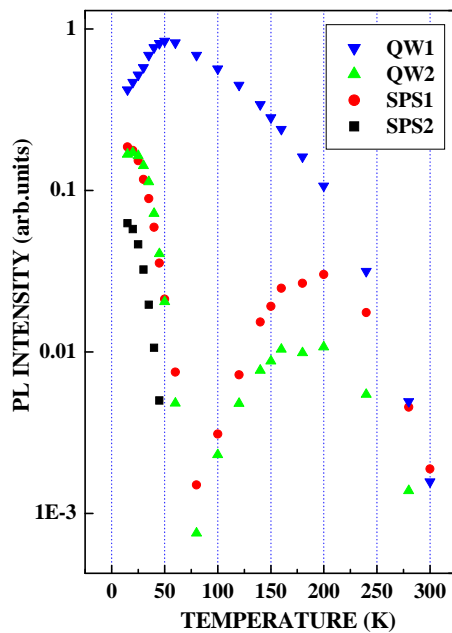


Fig. 6 Temperature dependence of the PL peak intensity for QW1, QW2, SPS1, and SPS2.

increasing temperature, exhibiting the maximum value around 180-200 K. Figure 6 shows the PL peak intensities of QW1, QW2, SPS1, and SPS2 on a logarithmic scale as a function of the temperature. The dependence of the PL intensities of QW1, QW2, SPS1, and SPS2 on the temperature can be interpreted in terms of the ambipolar vertical transport of carriers in SPS1 assisted by phonon scattering. The drastic increase of the PL intensity of QW1 with increasing the temperature from 15 to 60 K can be attributed to the efficient vertical transport of photoexcited carriers from the narrower QW2 to the wider QW1 mediated by the Bloch transport via the miniband states of SPS1. The restoration of the PL intensities for QW2 and SPS1 at temperatures above 140 K indicates that the carriers are thermally excited into QW2 and SPS1.

3.3 PL dynamics

For a more detailed understanding of the vertical transport in such semiconductor heterostructures which contain SPSs and additional single QWs providing recombination centres, time-resolved PL spectroscopy is a powerful tool to study the PL dynamic properties. In particular, the trapping and the detrapping processes of photoexcited carriers by the localized recombination centres in QW1 and QW2 can be studied in the pico-second time domain. Figure 7 shows spectrally integrated PL transients for the emission bands of QW1, QW2, and SPS1 at temperatures between 20 and 280 K, plotted on a semi-logarithmic scale. At 20 K, the PL rise of SPS1 is the fastest among the three PL bands, reaching the maximum value at 0.2 ns after the laser pulse ($t = 0$ ns), although its PL intensity is low. After the maximum in the time trace for SPS1, the PL intensities of QW1 and QW2 still continue to increase as shown in Fig. 7(a). This behaviour is interpreted as an efficient transfer of photoexcited carriers into the exciton states in QW1 and QW2 after the carriers have relaxed into the lowest miniband of SPS1 losing their excess energies via emission of phonons.

The PL transients of QW1, QW2, and SPS1 in Fig. 7(a) exhibit a bi-exponential decay, which usually indicates the coexistence of at least two recombination channels, e.g., due to free and localized excitons [24]. In this temperature regime, the fast PL decay component is attributed to radiative recombination of free excitons, while the slow PL decay is assigned to excitons bound to localized potential minima due to

well-width fluctuations. The lateral carrier transfer between the QW growth islands has been investigated previously by time-resolved PL spectroscopy. The PL dynamics are rigorously explained by a rate equation analysis [24, 28]. By bi-exponential fitting, the PL decay times of free excitons are estimated to be 0.9, 1.2, and 0.6 ns for QW1, QW2, and SPS1, respectively, at 20 K. The different values for QW1 and QW2 may reflect the impact of the increased oscillator strength due to quantum confinement on the radiative recombination lifetimes.

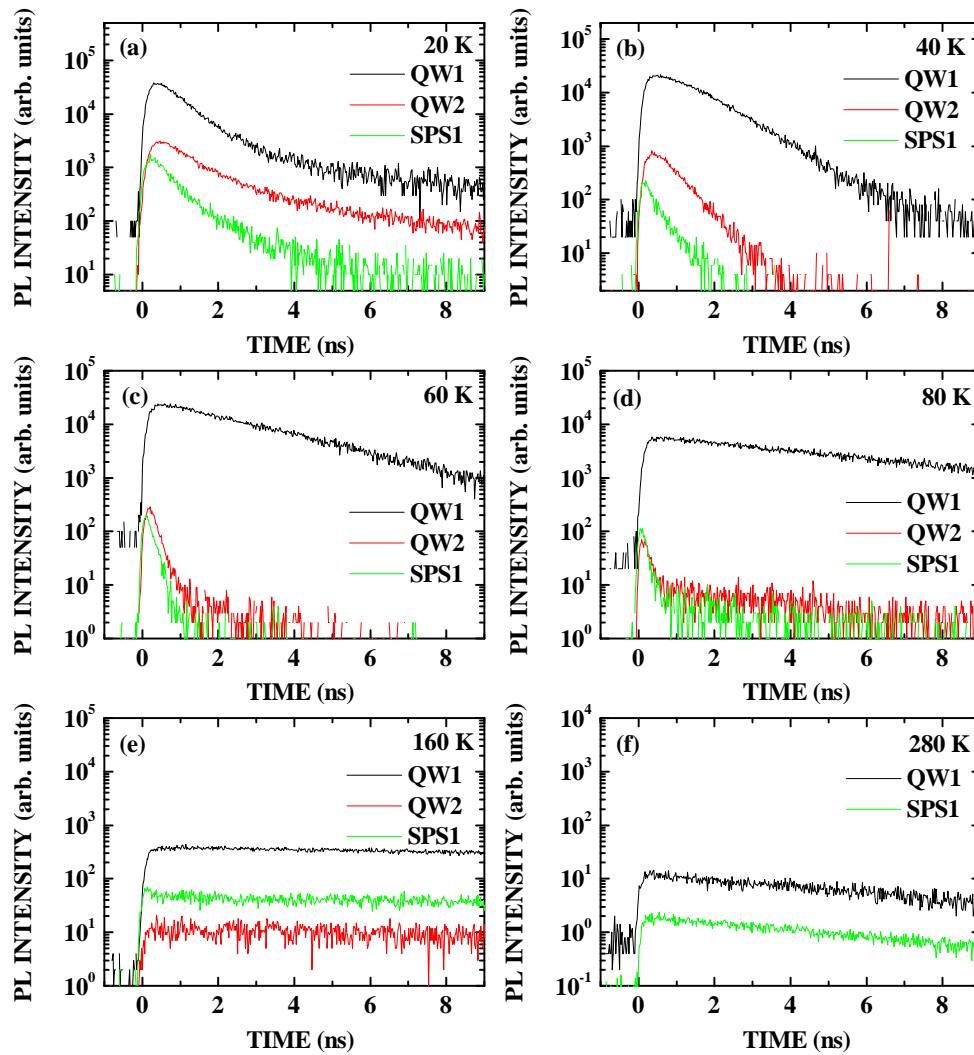


Fig. 7 PL transients as a function of time for QW1, QW2, and SPS1 at (a) 20 K, (b) 40 K, (c) 60 K, (d) 80 K, (e) 160 K, and (f) 280 K. The laser pulse position is located at $t = 0$ ns.

When the temperature is increased to 40 K, the bound excitons become delocalized. Therefore, the PL transients show a single-exponential decay time. The lifetimes increase with temperature in agreement with the linear temperature dependence expected for quasi-two-dimensional excitons [29]. However, note that the decay time of QW1 is considerably increased up to 8 ns at 80 K, while the ones of QW2 and SPS1 are drastically decreased to below 0.2 ns. The measured decay times for QW1, QW2, and SPS1 are plotted as a function of temperature in Fig. 8. Clearly, the linear temperature dependence obtained for QW1 is in good agreement with Feldmann et al. [29]. At least up to 50 K, the PL intensity of QW1 continues to increase due to the carrier supply from the QW2, SPS1, and SPS2, as shown in Fig. 6. Since in this temperature range the non-radiative recombination is of minor importance, the PL lifetime of QW1 is considered to be determined by the radiative recombination. On the other hand, the PL decay times for QW2 and SPS1 are found to be considerably decreased down to 0.18 and 0.16 ns, respectively, at 80 K. Taking into consideration the reduced PL intensities for QW2 and SPS1 as shown in Fig. 6, it is easily understood that their PL decay times are reduced as a result of the phonon-assisted carrier escape processes from the respective exciton states in QW2 and SPS1. That is, the carrier escape is a kind of non-radiative processes for excitons in QW2 and SPS1.

The significant increase of the PL decay time of QW1 in the temperature region between 50 and 140 K is accompanied by a decrease of its PL intensity, as shown in Fig. 6. This peculiar temporal behaviour may be interpreted as an increasing density of dark excitons with larger in-plane momenta. Furthermore, the excitons may be partially ionized so that the subbands are thermally populated by free carriers and an electron-hole plasma is formed [30, 31]. This conjecture is supported by the observation of high energy tails for the respective PL bands at temperatures above 80 K (see Fig. 5). Above 100 K, even a restoration of the PL signals from QW2 and SPS1 is observed as shown in Fig. 6, which we attribute to thermally activated detrapping of carriers from QW1 to QW2 and SPS1. At the same time, this thermalization leads to rather long decay times of several tens of ns at temperatures between 140 and 180 K. For a further temperature increase up to 280 K, the PL decay time decreases to 8 ns. At the same time, a much faster reduction of the PL intensities (see Fig. 6) is observed, which is assumed to be due to thermal activation of the non-radiative recombination processes by defects.

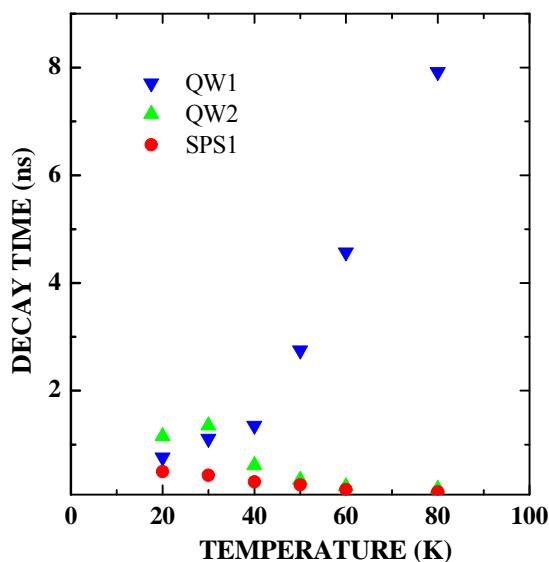
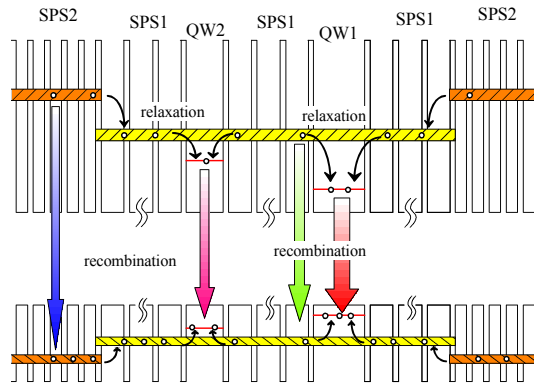


Fig. 8 PL decay time due to free excitons for QW1, QW2, and SPS1 as a function of temperature.

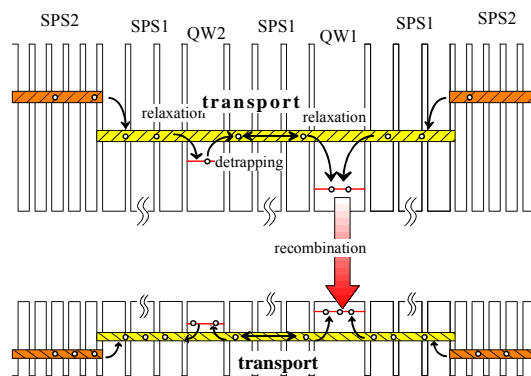
3.4 Vertical transport of photoexcited carriers

The vertical transport of photogenerated carriers/excitons has been studied in more detail discussing the dependence of the respective PL spectra on time and temperature. Three different temperature regimes are distinguished, as schematically illustrated in Fig. 9. At low temperatures [Fig. 9(a)] where carrier

(a)



(b)



(c)

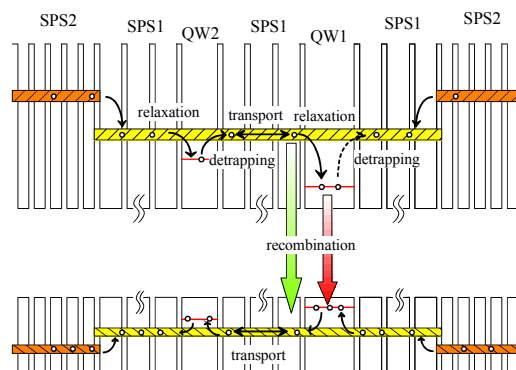


Fig. 9 Schematic potential diagrams for vertical transport between QW1 and QW2 in GaAs/AlAs SPS1: (a) 15-40 K, (b) 50-140 K, (c) 160-300 K. In the diagrams QW3 is omitted, since the lowest subband state is located above the minibands in SPS1.

cooling by emission of phonons dominates, the excess carriers, which are mainly photogenerated in the SPS2, are very rapidly transferred into QW1 and QW2. They are also captured by local potential minima within the miniband states in SPS1 where they form free and bound excitons. Since non-equilibrium populations at these exciton states are stable at low temperatures, they are only extinguished by radiative recombination processes. Therefore, their dynamics are basically determined by radiative recombination lifetimes of the excitons. Lateral transfer between the growth islands can also influence the energy dependent PL time behaviour within the inhomogeneously broadened exciton bands [25]. At slightly higher temperatures up to 50 K, the localized or bound excitons disappear and the free exciton dominates the PL spectral features, as confirmed by the linear temperature dependence of lifetime for QW1.

On the other hand, the non-equilibrium populations at the exciton states in QW2 and SPS1 become unstable at 30-50 K, because of phonon-assisted exciton scattering [32]. In particular, excitons in higher states of QW2 and SPS1 are detrapped and transferred into the lowest exciton state in QW1 via ambipolar Bloch-type vertical transport in SPS1. This exciton detrapping processes can be considered as a non-radiative recombination processes for the exciton populations in QW2 and SPS1. Thus, their lifetimes become very short as demonstrated in Fig. 8. This is in strong contrast to the case of QW1 where no exciton detrapping is possible between 20 and 50 K. This is the reason why the PL signals of QW2 and SPS1 completely disappear while the PL intensity of QW1 increases [see Fig. 9(b)].

When the temperature is further increased to 120-140 K, we observe the interesting temperature regime where the PL intensity of QW1 gradually decreases with temperature, though its decay time increases. This peculiar PL behaviour is explained by the increased density of dark excitons and the partial ionization of excitons. At even higher temperatures above 200 K [see Fig. 9(c)], photoexcited carriers tend to be in thermal equilibrium. Therefore, the emission band from the miniband states of SPS1 with the highest density of states dominates the PL spectra, while the PL band of QW1 with the lowest sub-band state is still intense since its population described by the Boltzmann distribution function is rather large.

4 Conclusion

The dynamics of vertical transport in a unique quantum heterostructure consisting of all-binary GaAs/AlAs SPSs with wide and narrow GaAs quantum wells have been investigated as a function of temperature by steady-state and time-resolved photoluminescence experiments. The optical characterization by PL and PLE spectroscopy shows well-defined exciton states in the enlarged quantum wells as well as in the SPSs. The temperature dependence of the PL spectra indicates that photoexcited carriers can be transferred from the narrower to the wider well via vertical Bloch-type miniband transport in the SPS, assisted by interactions with phonons. Redistribution of carrier population in the different wells by phonon scattering is directly evidenced by measuring the PL dynamics. Radiative recombination dynamics in the heterostructure are thus explored in the three different transport regimes; that is, tunnelling transport affected by irreversible carrier cooling into deep localization states, phonon-assisted activation and efficient miniband Bloch transport, and thermalization processes.

Acknowledgements The authors would like to thank K. Satoh, M. Matsuo, T. Ikemoto, M. Yamada, Y. Yamamoto, and T. Nogami for their experimental assistance.

References

- [1] K. Fujiwara and K. Ploog, *Appl. Phys. Lett.* **45**, 1222 (1984).
- [2] K. Fujiwara, J. L. de Miguel, and K. Ploog, *Jpn. J. Appl. Phys.* **24**, L405 (1985).
- [3] K. Fujiwara, H. Oppolzer, and K. Ploog, *Inst. Phys. Conf. Ser. No.74*: Chapter 5, 351 (1985).
- [4] J. Wagner, W. Stolz, J. Knecht, and K. Ploog, *Solid State Commun.* **57**, 781 (1986).
- [5] K. Ploog, Y. Ohmori, H. Okamoto, W. Stolz, and J. Wagner, *Appl. Phys. Lett.* **47**, 384 (1985).
- [6] Y. Tokuda, K. Fujiwara, and T. Nakayama, *Inst. Phys. Conf. Ser. No.79*: Chapter 12, 697 (1986).
- [7] Y. Tokuda, Y. N. Ohta, K. Fujiwara, and T. Nakayama, *J. Appl. Phys.* **60**, 2729 (1986).
- [8] S. Noda, K. Fujiwara, and T. Nakayama, *Appl. Phys. Lett.* **47**, 1205 (1985).

copyright line will be provided by the publisher

- 1 [9] K. Fujiwara, A. Nakamura, Y. Tokuda, T. Nakamura, and M. Hirai, Appl. Phys. Lett. **49**, 1193 (1986).
2 [10] H. T. Grahn (Ed.), *Semiconductor Superlattices: Growth and Electronic Properties* (World Scientific, Singa-
3 pore, 1995).
4 [11] K. Fujiwara, J. Optical and Quantum Electronics **22**, S99 (1990).
5 [12] B. Deveaud, J. Shah, T. C. Damen, B. Lambert, A. Chomette, and A. Regreny, IEEE J. Quantum Electron. QE-
6 **24**, 1641 (1988).
7 [13] F. Cappaso, K. Mohammed, and A. Cho, IEEE J. Quantum Electron. QE-**22**, 1853 (1986).
8 [14] S. Nagahama et al., Jpn. J. Appl. Phys. **39**, L647 (2000).
9 [15] S. Nakamura and G. Fasol, *The Blue Laser Diode* (Springer-Verlag, Berlin, 1997).
10 [16] R. Köhler et al., Appl. Phys. Lett. **82**, 1518 (2003).
11 [17] B. Rosam, K. Leo, L. Yang, and M. M. Dignam, Appl. Phys. Lett. **85**, 4612 (2004).
12 [18] A. Nakamura, K. Fujiwara, Y. Tokuda, T. Nakayama, and M. Hirai, Phys. Rev. **B34**, 9019 (1986).
13 [19] K. Fujiwara, N. Tsukada, T. Nakayama, and A. Nakamura, Phys. Rev. **B40**, 1096 (1989).
14 [20] M. Yamada, Y. Yamamoto, T. Ikemoto, T. Nogami, and K. Fujiwara, Proceedings of 11th International Semi-
15 conducting and Insulating Materials Conference, Canberra, Australia, 2000 (IEEE, New Jersey, 2001), pp.248-
16 251.
17 [21] A. Satake, T. Ikemoto, K. Fujiwara, L. Schrottke, R. Hey, and H. T. Grahn, Physica **E13**, 711 (2002).
18 [22] L. Schrottke, H. T. Grahn, and K. Fujiwara, Phys. Rev. **B56**, 13321 (1997).
19 [23] K. Fujiwara, K. Kanamoto, and N. Tsukada, Phys. Rev. **B40**, 9698 (1989).
20 [24] K. Fujiwara, H. Katahama, K. Kanamoto, R. Cingolani, and K. Ploog, Phys. Rev. **B43**, 13978 (1991).
21 [25] K. Fujiwara, H. T. Grahn, and K. H. Ploog, Phys. Rev. **B56**, 1081 (1997).
22 [26] K. Fujiwara and K.H. Ploog, Physica **B308-310**, 765 (2001).
23 [27] H. C. Casey and M. B. Panish in: *Heterostructure Lasers* (Academic Press, New York, 1978).
24 [28] M. Matsuo, K.Sasayama, T. Nogami, K. Satoh and K. Fujiwara, Proceedings of 11th International Semicon-
25 ducting and Insulating Materials Conference, Canberra, Australia, 2000 (IEEE, New Jersey, 2001), pp.244-247.
26 [29] J. Feldmann, G. Peter, E. O. Göbel, P. Dawson, K. Moore, C. Foxon, and R. J. Elliott, Phys. Rev. Lett. **59**,
27 2337 (1987).
28 [30] G. W. 't Hooft, W.A. J. A. An der Poel, L. W. Molenkamp, and C. T. Foxon, Phys. Rev. **B 35**, 8281 (1987).
29 [31] G. W. 'tHooft, M. R. Leys, and H. J. Talen-v. d. Mheen, Superlattices and Microstruct. **1**, 307 (1985).
30 [32] S. Machida, M. Matsuo, K. Fujiwara, J.R. Folkenberg, and J.M. Hvam, Phys. Rev. **B67**, 205322 (2003).
31
32
33
34
35
36
37
38
39
40
41
42
43
44
45
46
47
48
49
50
51
52